Theoretical Investigation of Entropy Generation in Axisymmetric Stagnation Point Flow of Nanofluid Impinging on the Cylinder Axes with Constant Wall Heat Flux and Uniform Transpiration

Zahmatkesh, Reza; Mohammadiun, Hamid*+; Mohammadiun, Mohammad;
Dibaee Bonab, Mohammad Hossein; Sadi, Meisam
Department of Mechanical Engineering, Shahrood Branch, Islamic Azad University,
Shahrood, I.R. IRAN

ABSTRACT: *Dimensionless temperature, Nusselt number, and entropy generation in stagnation flow of incompressible nanofluid impinging on the infinite cylinder with uniform suction and blowing have been presented in this study. The initial stream rate of the steady free stream is $k\bar{}$. A similar solution of Navier-Stokes and energy equations has been presented. These equations are simplified by implementing appropriate transformations introduced in this research. The governing equations are solved where the heat flux at the cylinder's wall is constant. All these solutions are acceptable for Reynolds numbers $Re=k\bar{}a^2/2\upsilon_f$ of 0.1-1000, various dimensionless surface diffusion $S=U_0 / k\bar{}a$, and specific volume fractions of nanoparticles where a is the cylinder radius and υ_f is the kinematic viscosity of the base fluid. The results show that for all Reynolds numbers, diffusion depth of radial and axial components of velocity field and wall shear stress increases as a result of the decline in nanoparticles volume fraction and growth in surface diffusion. Moreover, an increase in nanoparticles volume fraction and surface suction raises the heat transfer coefficient and Nusselt number. Also, the greatest amount of entropy generation is calculated.*

KEYWORDS: *Nanofluid, Stagnation flow; Similarity solution; Volume fraction; Entropy generation.*

INTRODUCTION

Nanofluids are fluids consisting of suspended solid nanoparticles of less than 100 nm size and 5 % volume fraction. This definition was first introduced by *Choi* [1]. The selection of suitable nanoparticles can improve fluid heat transfer compared with pure liquids. The nanofluids can be applied to improve the system's heat management in engineering applications, including heat transfer, micromechanics, air conditioning systems, and cooling facilities. In recent years, large numbers of numerical and experimental investigations have focused on nanofluids' convection heat transfer in different geometries.

Kuznetsov and Nield investigated free convection heat

transfer in the boundary layer of a laminar nanofluid analytically [2]. They merged the applied model for nanofluid with Brownian motion effects. In another research, *Kuznetsov* and *Nield* investigated thermal instability in a porous boundary layer saturated with nanofluid. Recently, *Khan* and *Pop* studied the boundary layer flow of nanofluid passing over an extended surface [4]. The relation of nanofluid's conduction coefficient with temperature was not taken into account in the models presented by Kuznetsov-Nield and Khan-Pop.

Generally, finding exact solutions for Navier-Stokes equations incorporates many complexities. This is because of the equations' nonlinearities which makes the application of the superposition theorem useless in this case, while it is very profitable in potential flow. However, in some specific cases, exact solutions are achievable for Navier-Stokes equations. Most of these solutions are related to the cases with advection terms, which are the nonlinear part of the problem, naturally eliminated. The first exact solution for the stagnation flow problem was introduced by *Hiemenz* [5], who achieved an ordinary differential equation. The two-dimensional stagnation flow over a flat surface was investigated in this solution.

After *Hiemenz*, *Homann* [6] obtained an exact solution for three-dimensional Navier-Stokes from axisymmetric stagnation flow over a flat plate. *Howarth* [7] and *Davey* [8] investigated the three-dimensional stagnation flow over a flat plate for nonaxisymmetric states. The first exact solution for axisymmetric stagnation flow over an infinite cylinder was presented by *Wang* [9]. In this solution, it is assumed that the cylinder is fixed with no rotation or axial movement and there are no flow passing over the surface and no surface suction and blowing. The flow is radially axisymmetric and perpendicular to the axis. *Gorla* [10-13] investigated the axisymmetric stagnation flow around the cylinder in a set of papers where the flow was assumed laminar in steady and transition states. The effects of uniform and harmonic axial movement of the cylinder were investigated in these papers. *Cunning et al.* [14] studied the effect of the cylinder's rotation with constant rotational speed for stagnation flow over the cylinder. The effect of uniform suction and blowing on the cylinder surface was also investigated in this study. *Takhar et al.* [15] studied the effect of unsteadiness in radially axisymmetric stagnation flow over the cylinder beside the effect of the cylinder's axial movement with variable velocity. *Saleh* and *Rahimi* [16-18]

introduced exact solutions for axisymmetric stagnation flow over an infinite cylinder as well as its heat transfer considering states with axial and rotational movement of the cylinder as a function of time. Also, *Abbasi* and *Rahimi* [19-22] presented exact solutions for three-dimensional stagnation flow and heat transfer of incompressible viscose fluid in transition state over a flat plate. *Mohammadiun* and *Rahimi et al.* [23-25] introduced self-similar solutions to analyze axisymmetric stagnation flow and its heat transfer over a cylinder's axis considering the compressibility effects of flow in a steady state.

Thermodynamics' second law is considered very applicable in heat transfer and analysis of flow field problems in different devices. So, the systems' best performance is when the generated entropy is minimum. Also, entropy generation is absolutely related to the system's reversibility. In thermal systems, the main resources of entropy generation are heat transfer, mass transfer, viscosity losses, electrical conduction, chemical reaction, and the simultaneous effects of mass and heat transfer [26-29]. On the other hand, exergy loss in thermodynamic systems is related to entropy variation in those systems. In this regard, as the generated entropy increases in a system, exergy loss promotes, and exergy efficiency can be calculated from dissipated entropy. Also, it has been found that operating fluids are substantially effective in a system's energy increase or decrease. This effect depends upon conduction coefficient, heat capacity, and other physical properties. *Mahmud et al.* investigated the entropy generation in combined convection heat transfer in a channel under the influence of a magnetic field [30]. *Aziz* investigated entropy generation in parallel flow between two surfaces under various boundary conditions [31]. Magnetic field effects and viscosity dissipation on entropy production in the fluid film were studied by *Aïboud-Saouli et al.* [32-33]. They also investigated entropy generation in viscoelastic hydromagnetic fluid flow [34]. Besides, *Rezaiguia et al.* investigated the effects of Prandtl and Eckert numbers on local entropy generation in forced convection heat transfer inside the boundary layer [35]. *Hirschfelder et al.* presented a general formulation for entropy generation in Newtonian incompressible flow [36]. Entropy generation in forced convection heat transfer accompanied by mass transfer in a two-dimensional channel has been analyzed by *San et al.* [37]. *Bianco et al.* presented a numerical solution to improve forced convection heat transfer for

turbulent flow inside a square channel under wall constant heat flux in the presence of water-Aluminum oxide and calculated the generated entropy [38]. *Rashidi et al.* computed the entropy generation in stagnation flow over a flat plate in porous media [39].

In the last 30 years, minimization of entropy generation has been the subject of much research including *Bejan* and *Ledezma* [40], *Lin* and *Lee* [41], and *Sasikumar* and *Balaji* [42]. *Rashidi et al.* investigated entropy generation in hydromagnetic flow over a porous disk with different physical properties in 2014 [43]. *Malvandi et al.* have recently investigated thermodynamics second law and heat transfer for the fluid flow passing over a flat plate [44]. Freidoonimehr and Rahimi presented an exact solution to calculate the entropy generation in nanofluid hydromagnetic flow over a plate that could expand or contract and included surface suction and blowing in a steady-state [45]. Heat and mass transfer effects in three-dimensional mixed convection flow of Eyring Powell over an exponentially stretching surface with convective boundary conditions have been investigated by *Bilal et al.* [49]. Recently *Nematollahzadeh et al.* have presented an exact analytical solution for the convective heat transfer equation from a semi-spherical fin. They compared exact solutions with numerical results such as the finite difference method and midpoint method with Richardson extrapolation (Midrich) [50].

Mohammadiun et al. proposed self-similar Solutions of radial stagnation point flow and heat transfer of a viscous, compressible fluid impinging on a rotating cylinder [52].

Combined heat and mass transfer and thermodynamic irreversibilities in the stagnation point flow of Casson rheological fluid over a cylinder with catalytic reactions and inside a porous medium under local thermal nonequilibrium have been investigated by *Alizadeh et al* [53]. *Nasir et al* [54] applied the similarity solution method to solve the momentum and energy equations in the stagnation point of unsteady incompressible fluid toward the stretching/ shrinking sheet. The momentum and forced convection heat transfer from a rotating isothermal cylinder in power-law fluids, confined in between two plane walls have been studied by *Thakur et al.* [55]. A numerical solution to the three-dimensional unsteady problem of impulsive stagnation-point flow with mixed convection heat transfer on a vertical cylinder that rotates at a constant angular velocity has been presented by *Bayat et al* [56].

Numerical simulation has been applied to investigate the pulsatile flow and heat transfer of a micropolar fluid in a Darcy-Forchhmeir porous channel with transpiration at the wall by *Ashraf et al* [57]. *Salawu et al.* [58] have presented a theoretical analysis of thermal stability and entropy generation of reactive hydromagnetic Powell-Eyring fluid flow in a fixed vertical channel with variable electrical and thermal conductivity. *Amirsom et al.* [59] presented a similar solution to governing equations for the magneto convective stagnation point flow of bionanofluid with melting heat transfer. *Madelatparvar et al.* [60] developed a numerical code based on the Finite Element Method (FEM) for numerical Study on parameters affecting the structure of scaffolds prepared by freeze-drying.

A mathematical model for the prediction of internal recirculation of complex impinging stream reactors has been presented by *Safaei et al* [61]. To study the choking phenomena in the granular flow in an industrial screw feeder a computational fluid dynamics analysis has been performed by *Zahoor et al.* [62]. *Habibi et al.* [63] investigated the viscosity uncertainty in the floating-axis fluid flow and heat transfer along a horizontal hot circle cylinder immersed in a cold Al_2O_3 water nanofluid.

In this research, the entropy generation rate is analyzed theoretically in nanofluid axisymmetric stagnation flow impinging on the cylinder with uniform surface suction and blowing which has not been considered in past studies. As shown in Fig. 1, flow in cylindrical coordinates (r, φ, z) is assumed correspondent with velocity components (u, v, w). The cylinder is infinite in length with a radius of a. The cylinder's wall is under constant heat flux. Flow over the cylinder is radially inward, gets the stagnation point, and forms the stagnation circle $(r=a \& z=0)$. Subsequently, a flow parallel to the cylinder's axis (in the z-direction) is created whose size depends on the distance from the stagnation circle. The fluid is assumed incompressible and viscose near the cylinder. The far-field flow was of the potential type and studied based on ideal flow equations.

The following items are some of the stagnation flow applications over a cylinder: the analysis of centrifugal machinery movement, production processes in chemical, petrochemical, and cement industries, heating and cooling procedures, Rocket engines' acceleration phases, activating and disabling industrial machines, industrial mixtures, industrial sieves, and other industrial oscillating machines. In the industry also the movement of colored

Table 1: Base- and nano- fluid properties [51].

value	parameter
0.6316 (W/m-k)	Base-fluid conductivity (k_f)
40 (W/m-k)	Nanoparticles conductivity (k_p)
4.181 (kJ/kg-K)	Base-fluid specific heat capacity ($C_{p,f}$)
0.765 (kJ/kg-K)	nanoparticles specific heat capacity ($C_{p,p}$)
987.6 (kg/m³)	Base-fluid density
3600 (kg/m³)	nanoparticles density
0.000538 (kg/m-s)	Base-fluid dynamic viscosity
44 Nm	Nanoparticles diameter (d_p)
0.384 Nm	Base-fluid molecular diameter (d_f)
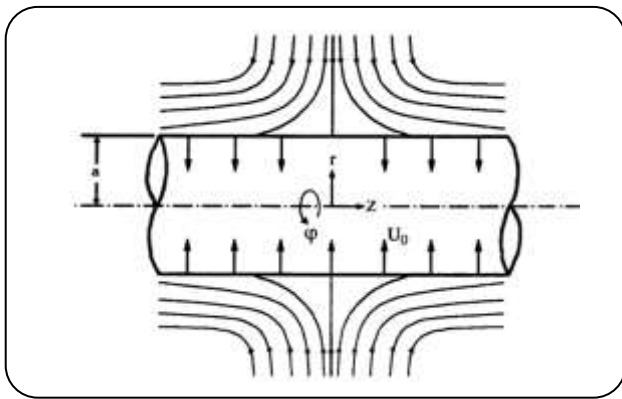
Fig. 1: Schematic diagram of radial stagnation flow over the infinite cylinder with uniform transpiration.

and polymeric fluids, fluid flow inside the bearings, microelectromechanical equipment, and micro fluids are usually described by low Reynolds number flow(Re<1).

THEORETICAL SECTION
Nanofluid properties
Aluminum oxide nanoparticles (γAl_2O_3) used in present research have the following properties:

density $\rho_u = 3600 \frac{Kg}{m^3}$, the average particle diameter of 44 nm and the other listed properties in Table 1.

Nanofluid density
In this research, the density of Aluminum oxide nanoparticles is assumed constant over the whole temperature domain, and the following equation is used to calculate the nanofluid density:

$$\rho_n = \left(1-\phi_v\right)\rho_f \times \phi_v \rho_p \tag{1}$$

Where n, f, and p indexes introduce nanofluid, base-fluid, and Aluminum oxide particles respectively and ϕ_v is the volume fraction of suspended particles in the fluid.

Dynamic viscosity of nanofluid
Nanofluid dynamic viscosity can be quantified by the present relation for two-phase mixtures.

Einstein introduced the Einstein formula to assess effective velocity [48]. The fluid contains a dilute suspension of spherical and small particles.

$$\mu_n = \mu_0 \left(1-2.5\phi_v\right) \tag{2}$$

This equation is applicable for low volume concentration of particles, less than 5%. There are different equations with their applications and restrictions to determine two-phase mixture equivalent viscosity. Results show that the Brinkman formula is not consistent with experimental data. Also, Brinkman has introduced the generalized form of the Einstein equation as follows:

$$\mu_n = \mu_0 \left(1-\phi_v\right)^{-2.5} \tag{3}$$

One of the most comprehensive equations for the calculation of nanofluid kinematic viscosity is the following equation presented by Corcione [46]:

$$\frac{\mu_n}{\mu} = \frac{1}{1-34.87\left(\frac{d_p}{d_f}\right)^{-0.3}\phi_v^{1.03}} \tag{4}$$

Where d_f is the equivalent diameter of one molecule of base-fluid calculated as below:

$$d_f = 0.1\left(\frac{6M}{N\pi\rho_{f0}}\right)^{\frac{1}{3}} \tag{5}$$

Where M is the base-fluid molecular weight, N is the Avogadro number and ρ_{f0} is the base-fluid density at $T_0=293k$. In the present research, the Corcione formula has been implemented to rewrite Navier-Stokes governing equations of nanofluid and energy equation.

Nanofluid conductivity
The following equation is suggested for the calculation of nanofluid conductivity [46]:

$$\frac{k_{eff}}{k_f} = 1+4.4Re_p^{0.4}Pr_{bf}^{0.66}\left(\frac{T}{T_{fr}}\right)^{10}\left(\frac{k_p}{k_f}\right)^{0.03}\phi_v^{0.66} \tag{6}$$

Pr_{bf} , Re_p are defined in the following equations:

$$Re_p = \frac{2\rho_{bf}k_b T}{\pi \mu_{bf}^2 d_p} \quad \& \quad Pr_{bf} = \frac{\mu_{bf}(c_p)_{bf}}{k_{bf}} \tag{7}$$

Covering equation

The steady Navier-Stokes and energy equations in cylindrical coordinates governing the axisymmetric flow are given by:

Continuity equation

$$\frac{\partial}{\partial r}(ru) + r\frac{\partial w}{\partial z} = 0 \tag{8}$$

Momentum equation in r direction

$$u\frac{\partial u}{\partial r} + w\frac{\partial u}{\partial z} = -\frac{1}{\rho_n}\frac{\partial P}{\partial r} + \upsilon_n \left(\frac{\partial^2 u}{\partial r^2} + \frac{1}{r}\frac{\partial u}{\partial r} - \frac{u}{r^2} + \frac{\partial^2 u}{\partial z^2} \right) \tag{9}$$

Momentum equation in the z-direction

$$u\frac{\partial w}{\partial r} + w\frac{\partial w}{\partial z} = -\frac{1}{\rho_n}\frac{\partial P}{\partial r} + \upsilon_n \left(\frac{\partial^2 w}{\partial r^2} + \frac{1}{r}\frac{\partial w}{\partial r} + \frac{\partial^2 w}{\partial z^2} \right) \tag{10}$$

Energy equation

$$\frac{1}{r}\frac{\partial}{\partial r}\left(rk_{eff}\frac{\partial T}{\partial r} \right) + \frac{\partial}{\partial z}\left(k_{eff}\frac{\partial T}{\partial z} \right) = \tag{11}$$

$$\left(\rho c_p \right)_n \left[u\frac{\partial T}{\partial r} + w\frac{\partial T}{\partial z} \right]$$

Boundary conditions

$$r = a: \quad u = -U_0, w = 0 \tag{12}$$

$$r \rightarrow \infty: \quad u = -\bar{k}\left(r - \frac{a^2}{r} \right) \& \frac{\partial u}{\partial r} = -\bar{k}, \quad w = 2\bar{k}z \tag{13}$$

$$r = a: \quad \frac{\partial T}{\partial r} = -\frac{q_w}{k_{nf}} \tag{14}$$

$$r \rightarrow \infty: \quad T = T_\infty$$

Where k_{nf} is the nanofluid conduction coefficient and, q_w is the specified heat flux over the cylinder's wall. Also T_∞ is the free stream temperature or far-field temperature of the fluid that is assumed constant.

Utilizing suitable similarity variables, the number of variables in governing equations is reduced. Regarding inviscid solutions presented in Eq. (13) and multiplying these equations in appropriate transformation functions, the following equations are presented to reduce Navier-Stokes equations to dimensionless similarity ones [9]:

$$u = -\bar{k}\frac{a}{\sqrt{\eta+1}}f(\eta), w = 2\bar{k}f'(\eta)z, P = \rho_n \bar{k}^2 a^2 p \tag{15}$$

In above equations ( )' introduces derivative with respect to variable η which is:

$$\eta = (\frac{r}{a})^2 - 1 \tag{16}$$

Eq. (15) satisfies the continuity equation automatically and by substituting these equations in the momentum equation in z and r directions, an ordinary differential equation is obtained to find f:

$$(\eta+1)f''' + f'' + Re_n\left[1 - (f')^2 + ff'' \right] = 0 \tag{17}$$

Nanofluid's Reynolds number in Eq. (17) is:

$$Re_n = \beta\frac{\bar{k}a^2}{2\upsilon_f} \tag{18}$$

$$\beta = \left[1 - 34.87\left(\frac{d_p}{d_f} \right)^{-0.3} \varphi_v^{1.03} \right]\left(1 - \varphi_v + \varphi_v\frac{\rho_p}{\rho_f} \right) \tag{19}$$

The required boundary conditions to solve Eq.(17) are obtained from Eqs (12) and (13):

$$\eta = 0: \quad f = S = \frac{U_0}{\bar{k}a}, \quad f' = 0 \tag{20}$$

$$\eta \rightarrow \infty: \quad f' = 1$$

To transfer energy equation, the dimensionless variable of $\theta(\eta)$ is used:

$$\theta(\eta) = \frac{T(\eta) - T_\infty}{\dfrac{aq_w}{2k_{bf}}} \tag{21}$$

In this state, boundary conditions presented in Eq. (14) are defined as below:

$$\eta = 0: \quad -\frac{k_{nf}}{k_{bf}}\theta'(0) = 1 \tag{22}$$

$$\eta \rightarrow \infty: \quad \theta = 0$$

Simplifying Eq. (11), the energy equation will be:

$$\left\{1+\Gamma\varphi_v^{0.66}\,Pr_{bf}^{0.66}[T_\infty+\frac{aq_w}{2k_{bf}}\theta]^{10.4}\right\}\times \tag{23}$$

$$[(\eta+1)\theta''+\theta']+10.4[T_\infty+\frac{aq_w}{2k_{bf}}\theta]^{9.4}\times$$

$$\frac{aq_w}{2k_{bf}}\Gamma\varphi_v^{0.66}\,Pr_{bf}^{0.66}(\eta+1)(\theta')^2+$$

$$\left\{1-\varphi_v+\varphi_v[\frac{(\rho c_p)_p}{(\rho c_p)_f}]\right\}Re_{bf}\,Pr_{bf}\,f\theta'=0$$

Where $\Gamma=4.4(\dfrac{2\rho_{bf}K_b}{\pi\mu_{bf}^2 d_p})^{0.4}\dfrac{1}{T_{fr}^{10}}(\dfrac{k_p}{k_f})^{0.03}$

The following equations are utilized in calculating convection heat transfer coefficient and Nusselt number, while constant heat flux is applied on the cylinders' wall:

$$\theta(0)=\frac{T_w-T_\infty}{\dfrac{aq_w}{2k_{bf}}}\,\&\,h=\frac{q_w}{T_w-T_\infty}\rightarrow \tag{24}$$

$$Nu=\frac{ha}{2k_{bf}}=\frac{1}{\theta(0)}$$

Eqs (17) and (23) with their boundary conditions are solved simultaneously by the finite difference method and the Three-Diagonal Matrix Algorithm (*TDMA*). The results will be discussed in the following sections.

Shear stress over the cylinder wall

The following equation is used to calculate effective shear stress over the cylinder wall:

$$\sigma=\mu\left[\frac{\partial w}{\partial r}\hat{e}_z\right]_{r=a} \tag{25}$$

To calculate the shear stress, $\frac{\partial w}{\partial r}$ is transformed using the chain rule:

$$\frac{\partial w}{\partial r}=\frac{\partial w}{\partial\eta}\frac{\partial\eta}{\partial r}=(2\bar{k}f''z)\frac{2r}{a^2} \tag{26}$$

With r=a and $\eta=0$, shear stress is calculated from the following equation:

$$\sigma=\mu_n\left[2\bar{k}f''(0)z\right]\frac{2}{a}\Rightarrow\frac{\sigma a}{4\mu_n\bar{k}z}=f''(0) \tag{27}$$

Stream function

To give a better description of the fluid flow, streamlines are drawn in r-z plane. In this regard, Stokes dimensionless stream function $\hat{\psi}$ is defined:

$$\hat{\psi}=\frac{\psi}{ka^3}=f(\eta)\left(\frac{z}{a}\right) \tag{28}$$

The velocity components are rewritten using stream function:

$$\begin{cases}u=-\dfrac{1}{r}\dfrac{\partial\psi}{\partial z}\\[2mm]w=\dfrac{1}{r}\dfrac{\partial\psi}{\partial r}\end{cases} \tag{29}$$

Calculation of entropy generation

Entropy generation is discussed in two different approaches. The first calculates local entropy generation in each point of the system and in the second one, total entropy generation (average value) can be obtained by integrating the local entropy distribution function over the control volume.

Local entropy generation is calculated in cylindrical coordinates by the following equations [47]:

$$\dot{S}_{gen}'''=\frac{k}{T^2}\left[\left(\frac{\partial T}{\partial r}\right)^2+\left(\frac{1}{r}\frac{\partial T}{\partial\theta}\right)^2+\left(\frac{\partial T}{\partial z}\right)^2\right]+ \tag{30}$$

$$\frac{\mu}{T}\left\{\begin{array}{l}2\left[\left(\dfrac{\partial u}{\partial r}\right)^2+\dfrac{1}{r^2}\left(\dfrac{\partial v}{\partial\theta}+u\right)^2+\left(\dfrac{\partial w}{\partial z}\right)^2\right]+\\[3mm]\left(\dfrac{\partial v}{\partial z}+\dfrac{1}{r}\dfrac{\partial w}{\partial\theta}\right)^2+\left(\dfrac{\partial w}{\partial r}+\dfrac{\partial u}{\partial z}\right)^2+\\[3mm]\left(\dfrac{1}{r}\dfrac{\partial u}{\partial\theta}+r\dfrac{\partial}{\partial r}\left(\dfrac{v}{r}\right)\right)^2\end{array}\right\}$$

Looking at the above equations, entropy generation depends on two factors, first one id related to heat conductivity where finite temperature difference produces entropy and the second factor is related to frictional irreversibility of viscose fluid which depends upon the velocity gradient. As dimensionless results are preferable, the entropy generation rate $(\dot{S}''')$ is divided to $\dot{S}'''=\frac{k_f\Delta T}{a^2 T_\infty}$ and the final result is expressed as $N_G=\frac{\dot{s}'''}{\dot{s}_0'''}$.
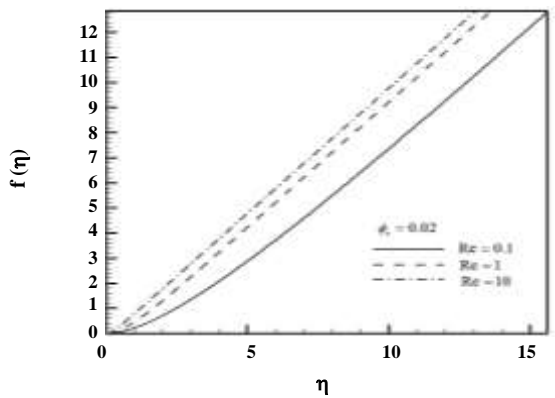
Fig. 2: Variation of $f(\eta)$ with respect to η in $\phi_v = 0.02$ for different Reynolds numbers.

Fig. 3: Variation of $f'(\eta)$ with respect to η in Re = 1000.

RESULTS AND DISCUSSION

Here, the results of solving differential Eqs (17) and (23) for different Reynolds numbers and selected values of volume fractions are presented and the entropy generation rate is calculated after the determination of velocity field and dimensionless temperature.

A typical $f(\eta)$ curve with respect to η for the volume fraction of ($\phi_v = 0.02$) and selected Reynolds number is presented for the rigid wall in Fig. 2.

As shown in the figure, diffusion depth of fluid velocity radial component field goes up with an increase in Reynolds number. The reason can be the fact that fluid radial inertia increases as the Reynolds number grows. In other terms, the flow field radial component grows with an increase in the diffusion of fluid radial momentum.

The effect of nanoparticles volume fraction on function $f'(\eta)$ in S=0, Re=1000 is indicated Fig. 3.

The results of the presented solution in $\phi_v = 0$ (for base-fluid) have shown good consistency with Wang's solution results [9]. Increasing nanoparticles volume fraction, diffusion depth of velocity field axial component declines. In other words, nanoparticle injection to base-fluid decreases fluid inertia. Axial velocity demotes a reduction in fluid axial motion. The results point out that the highest axial component is defined in base-fluid.

A typical $f'(\eta)$ curve with respect to η for S=0, $\phi_v = 0.02$ and selected Reynolds numbers are depicted in Fig. 4. As expected, velocity boundary layer thickness diminishes with growth in Reynolds number which increases the slope of velocity distribution profile in $\eta = 0$. As a result velocity gradient goes up over the cylinder's wall. The same results can be obtained for other nanoparticles volume fractions.
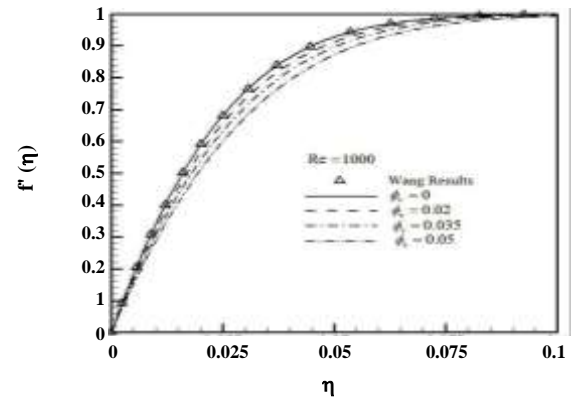
Wall shear stress with respect to Reynolds number in different nanoparticles volume fractions for rigid cylinder without surface suction or blowing is Fig. 5. Based on these curves, it is concluded that an increase in nanoparticles volume fraction diminishes wall shear stress. Because this increase reduces the slope of velocity distribution profiles and velocity gradient over the surface. It declines shear stress over the cylinder wall. Also, Equation (27) states that dimensionless shear stress over the surface is equal to $f''(0)$ which defines the slope of the tangent line to f' curves in $\eta = 0$. According to Fig. 3, the slope of tangent lines to f' curves and subsequently dimensionless shear stress reduces with an increase in nanoparticles weight fraction.

A typical curve of dimensionless temperature distribution (θ) with respect to η is presented in Fig. 6. Cylinder's wall is under constant heat flux. As expected, with an increase in Reynolds number, fluid momentum grows, and with a growth in diffusion depth of fluid momentum, not only the heat boundary layer's thickness but also surface dimensionless temperature decrease.

The effect of nanoparticles volume fraction on dimensionless temperature θ curves are shown in Fig. 7 while constant heat fluxes are applied on the cylinder's wall without any surface suction or blowing. According to these curves, for zero-valued volume fraction ($\phi_r = 0$), *Gorla*'s [12] results are reproduced and the suggested method is validated where with an increase in nanoparticles volume fraction, dimensionless temperature gradient decreases over the surface and conduction coefficient inversely goes up. As the increase in conduction coefficient is higher than the decrease in a dimensionless temperature gradient, the convection heat transfer coefficient goes up.
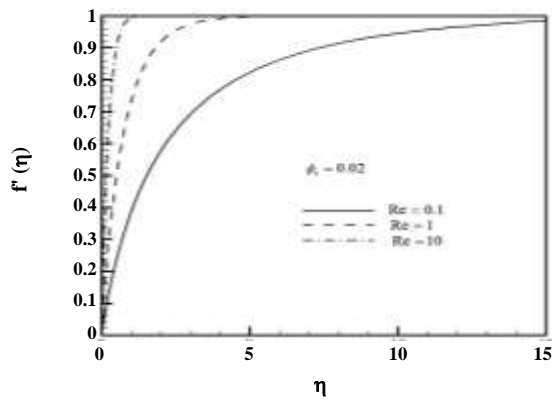
Fig. 4: Variation of f'(η) with respect to η in φᵥ = 0.02 for different Reynolds numbers.
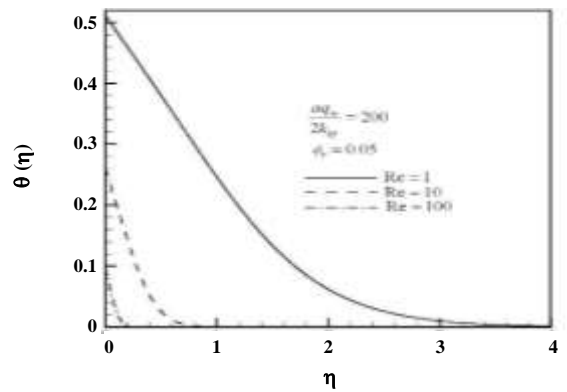

Fig. 6: Dimensionless temperature θ curves for various wall constant heat fluxes in different Reynolds numbers.
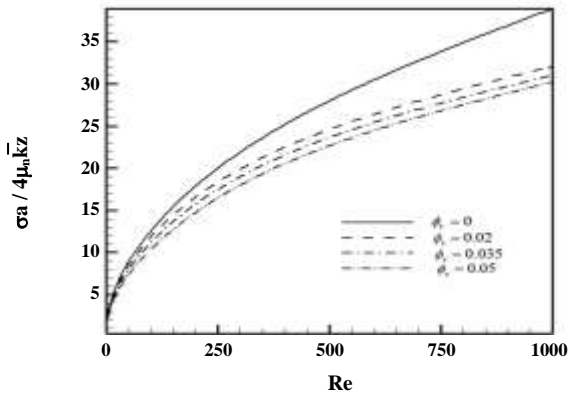

Fig. 5: Variation of cylinder's wall shear stress with respect to Reynolds number for different nanoparticles volume fractions.
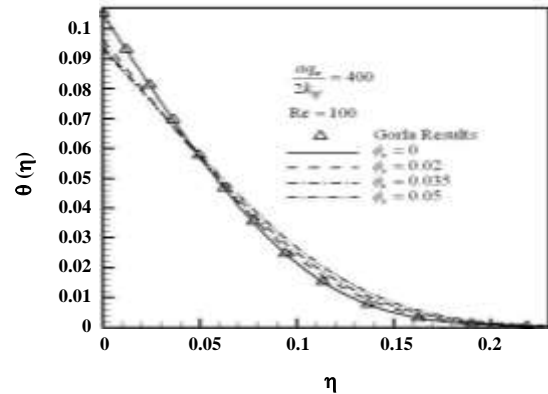

Fig. 7: Effect of nanoparticles volume fraction on dimensionless temperature.

The effect of nanoparticles volume fraction on Nusselt number when cylinder's wall is under constant heat flux is indicated in Fig. 8. Nusselt number with respect to Reynolds number in different volume fractions is plotted in these curves. With an increase in nanoparticles volume fraction, dimensionless temperature $[\theta(0)]$ over surface declines. As Nusselt number is inversely proportional to dimensionless temperature over a surface according to Eq. (24), Nusselt number has raised improving conduction coefficient.

The effect of surface suction on streamlines is shown in Figs. 9 and 10. The streamlines are plotted in Re=10, Re=100, ($\phi_v = 0.02$) and surface suction values of S=0, 0.5, 1, and with an increase in surface suction streamlines drawn toward the cylinder, more surface suction results in fewer stream lines' widths.

A typical $f(\eta)$ curve with respect to η for volume fraction ($\phi_v = 0.02$) and Re=0.1 and selected values for surface suction and blowing is presented in Fig. 11. As it is found from the figure, with an increase in surface suction, $f(\eta)$ promotes meaning that diffusion depth of velocity field radial component grows. The reason is that growth in surface suction raises fluid inertia in the fluid motion toward the cylinder's surface and causes an increase in velocity field radial component. But, as expected, surface blowing acts completely the reverse which means: an increase in surface blowing reduces $f(\eta)$ resulting in a drop in velocity field radial component. Because motion inertia for the fluid blown is absolutely in the opposite direction to the fluid jet getting close to the surface. Obviously, fluid radial motion decreases in this case. It can be shown that similar results are obtained
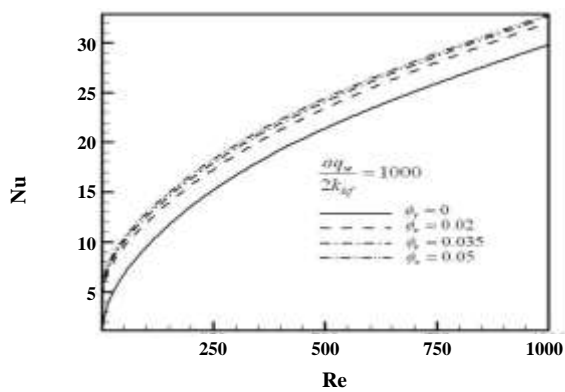
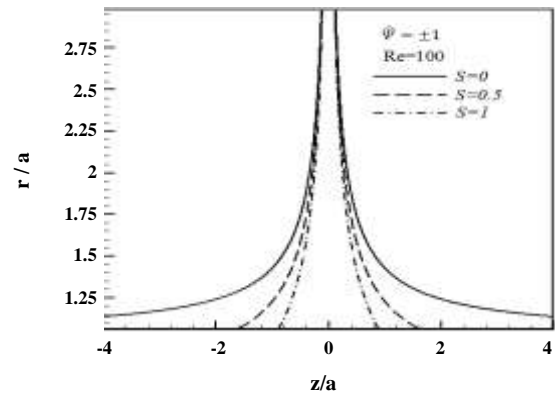**Fig. 8: Effect of nanoparticles volume fraction on Nusselt number.**

Fig. 10: Streamlines $\widehat{\Psi} = \pm 1$ for different values of surface suction in Re=100.
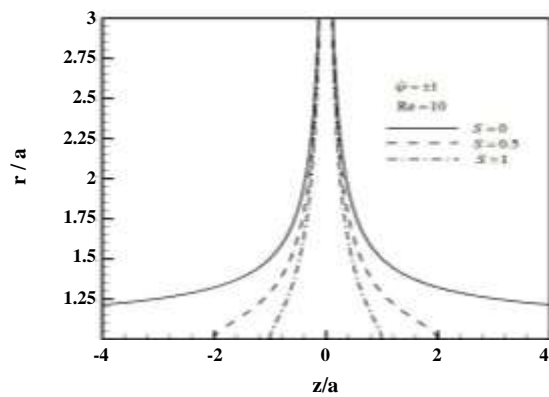

Fig. 9: Streamlines $\widehat{\Psi} = \pm 1$ for different values of surface suction in Re=10.
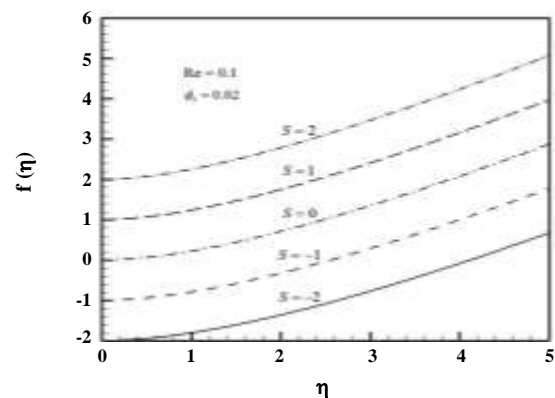

Fig. 11: Variation of $f(\eta)$ with respect to η in $(\phi_v = 0.02)$ and Re=0.1 for different suction and blowing values applied constantly over the surface.

for other Reynolds numbers. In all cases, the promotion of the Reynolds number results in an increase in diffusion depth of velocity field radial component due to fluid inertia growth.

Effect of suction and blowing on $f'(\eta)$ in $(\phi_v = 0.02)$ and for selected values of Reynolds number is shown in Figs. 12 and 13 respectively. As indicated, $f'(\eta)$ promotes an increase in suction over the cylinder's surface for all Reynolds numbers. In other terms, surface suction growth raises velocity field axial component, because it increases fluid momentum. In this case, surface blowing acts completely the reverse which means: an increase in surface blowing reduces $f'(\eta)$ resulting in a drop in velocity field radial component. Because fluid blowing in the opposite direction reduces the striking fluid jet momentum which results in a decrease in velocity field

axial component. In all cases, surface suction reduces the boundary layer's thickness causing an increase in surface velocity gradient. Reversely, surface blowing promotes the boundary layer's thickness causing growth in velocity gradient over the cylinder's surface.

A typical shear stress curve is plotted as a function of the Reynolds number in Fig. 14. Dimensionless surface suction is assumed S=0,1,2. As expected, surface suction affects the shear stress over the cylinder's surface substantially and surface suction increase raises shear stress over the surface. Because an increase in surface suction reduces the boundary layer's thickness resulting in growth in the slope of velocity distribution profiles. In other words, the velocity gradient goes up over the surface. As shear stress is directly proportional to velocity gradient, surface suction increase promotes shear stress.
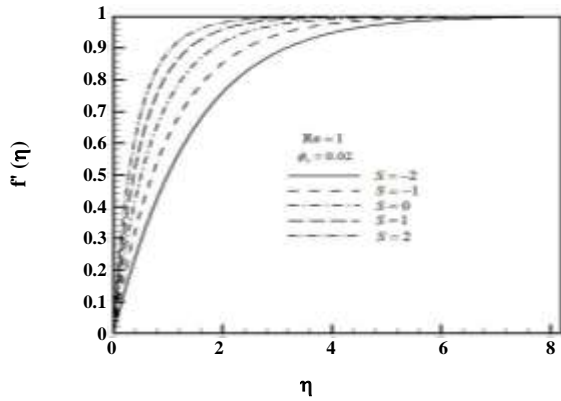
Fig. 12: Variation of $f'(\eta)$ with respect to η in $(\phi_v = 0.02)$ and Re=1 for different suction and blowing values applied constantly over the surface.
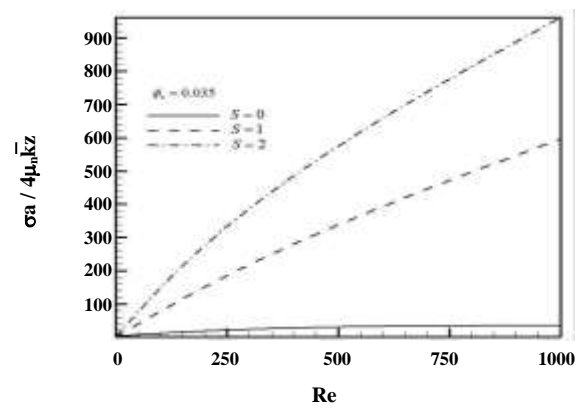

Fig. 14: Surface shear stress variation with respect to Reynolds number in $(\phi_v = 0.035)$ for different uniform surface suction values.
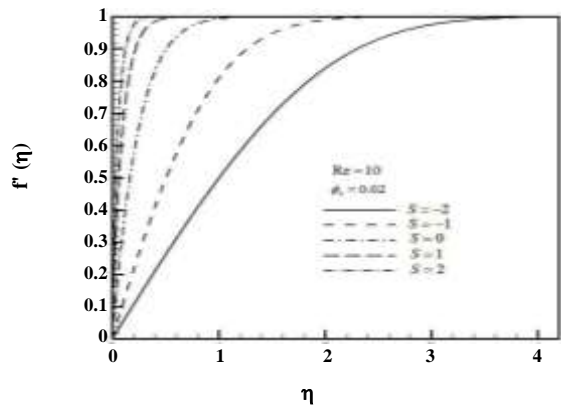

Fig. 13: Variation of $f'(\eta)$ with respect to η in $(\phi_v = 0.02)$ and Re=10 for different suction and blowing values applied constantly over the surface.
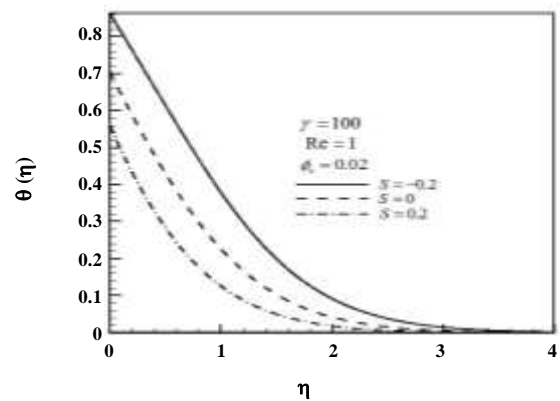

Fig. 15: Simultaneous effect of suction and blowing on dimensionless temperature $\theta(\eta)$ in Re=1.

Simultaneous effect of suction and blowing on dimensionless temperature $\theta(\eta)$ is investigated in Figs (15) and (16). As seen, this affects suction reversely. Because with an increase in suction, wall temperature diffusion depth rises in the fluid around the wall. So, the thermal boundary layer's thickness grows and surface blow adds up to surface temperature.

Variation of Nusselt number with respect to Reynolds number with constant heat flux over the wall and in volume fraction of $(\phi_v = 0.035)$ is shown in Fig. 17. If the cylinder's wall is under constant heat flux, the Nusselt number is proportional to inverse dimensionless temperature over the surface. As surface suction increase and diminishes dimensionless temperature over the cylinder surface, the Nusselt number goes up.

The effect of volume fraction on entropy generation rate with the wall under constant heat flux and uniform surface suction is represented in Figures (18) and (19). Very close to the surface, base-fluid entropy $(\phi_v = 0)$ is more than nanofluid entropy. The reason is that fluid momentum is more than nanofluid momentum which results in an increase in velocity field radial component as well as velocity gradient. In other words, the frictional irreversibility growth rate is more than thermal irreversibility resulting from wall heat flux which increases total entropy. The curves follow the same trend for volume fractions $(\phi_v = 0.02.0.035.0.05)$.

At first and because of frictional irreversibility reduction, the entropy generation rate declines with growth in volume fraction. Getting far away from the surface,
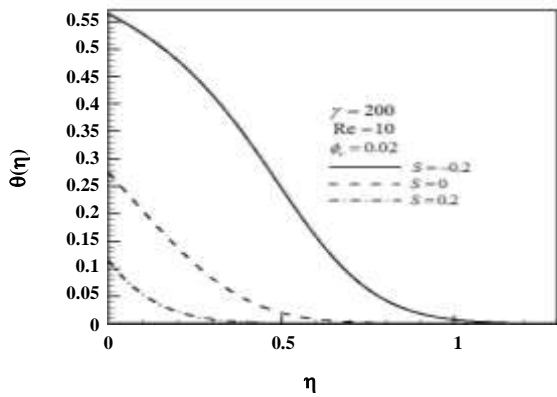
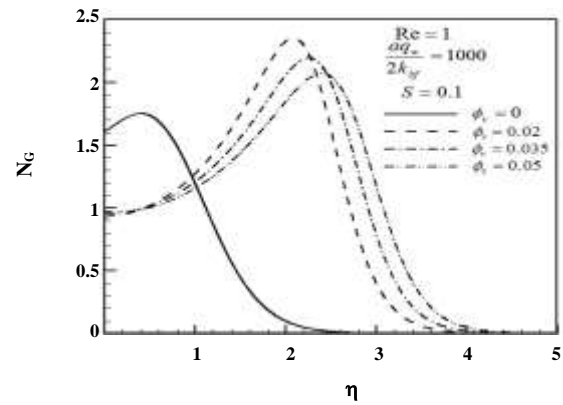**Fig. 16: Simultaneous effect of suction and blowing on dimensionless temperature $\theta(\eta)$ in Re=100.**

Fig.18: Entropy generation rate curves with respect to η in Re=1 for different volume fractions.
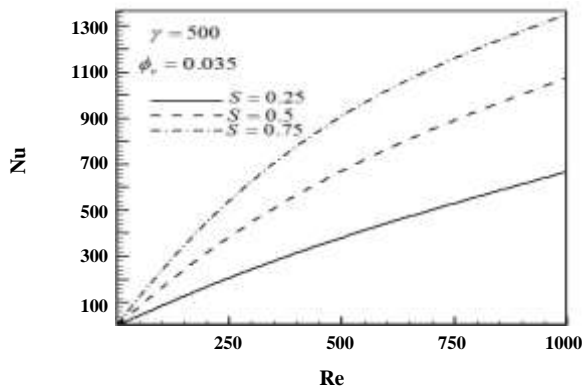

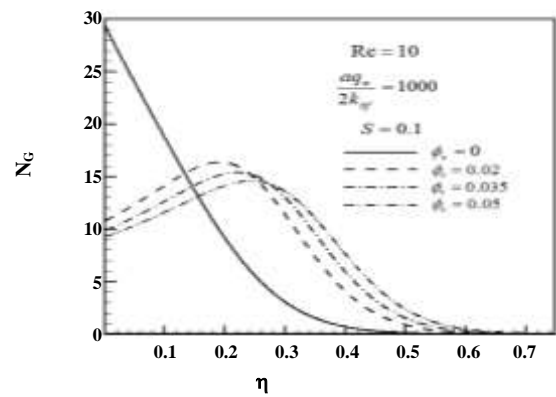**Fig. 17: Effect of surface suction on Nusselt number.**

Fig. 19: Entropy generation rate curves with respect to η in Re=10 for different volume fractions.

velocity gradients decrease and the effect of frictional irreversibility would become substantially less than thermal irreversibility. As predicted, with an increase in nanofluid volume fraction, thermal diffusion and heat transfer go up, entropy generation for nanofluid gets more than base-fluid and this continues as the volume fraction proceed to grow. This entropy generation continues to the point where substantial energy diffusion is found from the surface to the fluid and the velocity gradient is not zero. But the results also indicate that far from the surface, a reduction in velocity gradients and energy diffusion results in a less entropy generation rate and it's approaching zero.

As shown in Figs. 18 and 19, entropy is maximum in a specific radial distance from the cylinder's surface. This value is affected by fluid temperature, dynamic viscosity, conduction coefficient, velocity gradient, and temperature gradient. Maximum entropy and corresponding location are stated in Tables 2 to 4.

The effect of surface suction and blowing on entropy generation rate is shown in Figs. 20-22. According to the Figures, in areas close to the surface where surface suction has reduced thermal and hydrodynamic boundary layers' thickness, with an increase in temperature and velocity gradients, thermal as well as frictional entropy goes up simultaneously and entropy generation rate grows significantly, while surface blowing gets hot boundary layer away from the surface and promote thermal and hydrodynamic boundary layers' thickness. This increase in thickness reduces temperature and velocity gradients as well as thermal and frictional entropy which demotes the total entropy generation rate.

Table 2: Maximum entropy generation rate and its location in $\phi_v = 0.02$ and $\frac{aq_w}{2K_{bf}} = 1000$.

Re	η_{max}	$N_{G\ max}$
1	2.231	2.296
10	0.352	14.117
50	0.0985	43.086
100	0.056	68.823
250	0.0266	126.652
500	0.0153	196.914
1000	0.0082	301.658

Table 3: Maximum entropy generation rate and its location in $\phi_v = 0.035$ and $\frac{aq_w}{2K_{bf}} = 1000$.

Re	η_{max}	$N_{G\ max}$
1	2.404	2.146
10	0.381	13.49
50	0.1076	41.404
100	0.0618	66.064
250	0.029	121.08
500	0.0168	188.790
1000	0.0096	289.732

Table 4: Maximum entropy generation rate and its location in $\phi_v = 0.05$ and $\frac{aq_w}{2K_{bf}} = 1000$.

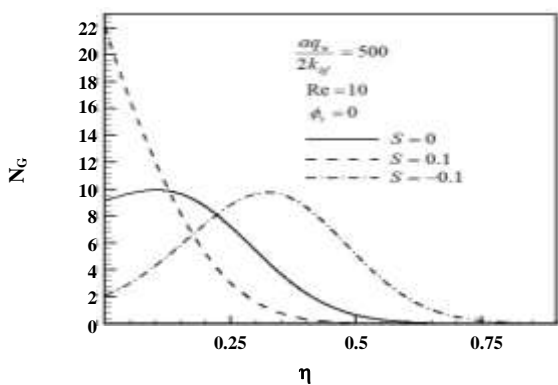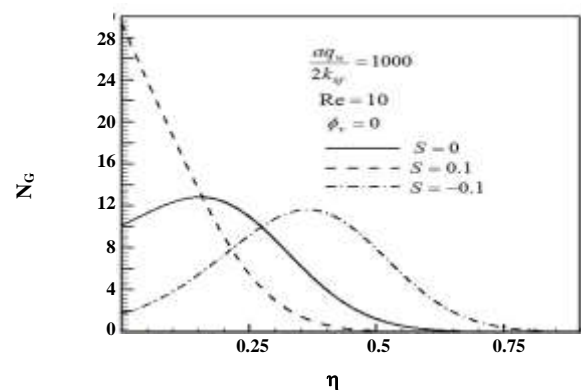| Re	η_{max}	$N_{G\ max}$
1	2.547	2.0273
10	0.405	12.917
50	0.1153	39.785
100	0.0667	63.44
250	0.0323	116.144
500	0.0185	181.11
1000	0.0104	278.273

Fig. 20: Entropy generation rate curves with respect to η for different surface suction and blowing.

Fig. 21: Entropy generation rate curves with respect to η for different surface suction and blowing.
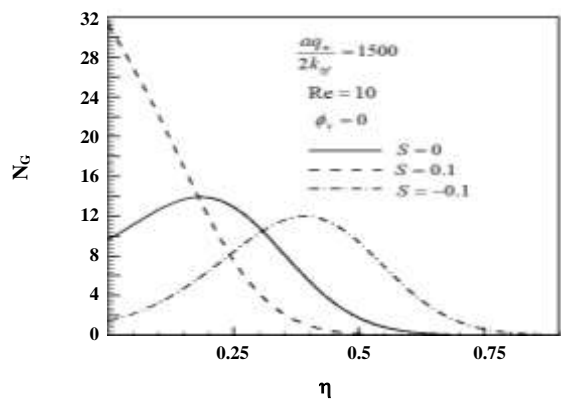
         Research Article

Fig. 22: Entropy generation rate curves with respect to η for different surface suction and blowing.

CONCLUSIONS

Similarity solution of nanofluid axisymmetric flow impinging on a cylinder, its heat transfer, and entropy generation have been presented in the current study. A system of partial differential equations was transformed to ordinary differential equations based on proper change of variables and transformation functions. The differential equations were solved by implementing the Thomas algorithm (TDMA) after discretization by the finite difference method. All these results were presented for Reynolds numbers of 0.1 to 1000 and different nanoparticles volume fractions. They indicate that increase in nanoparticle volume fraction reduces velocity field radial and shear stress axial components over the cylinder's wall. While conduction coefficient and Nusselt number go up. In all cases studied, the entropy generation rate has an increasing trend initially. Then after getting to the peak and far from the surface, it tends to zero as energy diffusion and velocity gradients decline.

Nomenclature

α	Cylinder radius, m
$C_{p,f}$	Base-fluid specific heat capacity, kJ/kg.K
$C_{p,p}$	Nanoparticles specific heat capacity, kJ/kg.K
d_f	The equivalent diameter of base-fluid molecules, m
d_p	The equivalent diameter of nanoparticles molecules, m
f	Dimensionless function defining velocity field
k_{eff}	Nanofluid conduction coefficient, W/m.K
$\bar{k}$	Velocity field axial component, m/s
p	Fluid pressure, N/m^2
P	Dimensionless pressure
r, z	Cylindrical coordinates, r,z
Re	Base-fluid's Reynolds number
Re$_n$	Nanofluid's Reynolds number
T	Temperature, K
U	Velocity field radial component, m/s
W	Velocity field axial component, m/s
η	Similarity variable
θ	Dimensionless temperature
μ	Base-fluid dynamic viscosity, kg/m.s
μ_n	Nanofluid dynamic viscosity, kg/m.s
υ_f	Base-fluid kinematic viscosity, m^2/s
υ_n	Nanofluid kinematic viscosity, m^2/s
ρ_f	Base-fluid density, kg/m^3
ρ_P	Nanoparticles density, kg/m^3
σ	Shear stress, N/m^2
ϕ_v	Volume fraction

REFERENCES

[1] Choi S.U.S., Eastman J.A., "Enhancing Thermal Conductivity of Fluid with Nanoparticles", *ASME Int. Mech. Eng. Cong. Expo.*, November 12-17, San Francisco, CA (1995).

[2] Kuznetsov A.V., Nield D.A., Natural Convection Boundary-Layer Flow of a Nanofluid Past a Vertical Plate, *Int. J. Thermal Sci.*, **49(2)**: 243–247 (2010).

[3] Kuznetsov A. V., Nield D.A., Thermal Instability in a Porous Medium Layer Saturated by a Nanofluid: Brinkman Model, *Transp. Porous Media*, **81(3)**: 409–422 (2010).

[4] Khan W.A., Pop I., Boundary-Layer Flow of a Nanofluid Past a Stretching Sheet, *Int. J. Heat Mass Transfer*, **53(11-12)**: 2477–2483 (2010).

[5] Hiemenz K., Die Grenzchicht an Einem in Den Gleichformingen Flussigkeitsstrom Eingetauchten Geraden Kreiszylinder, *Dinglers Polytechn. Journal,* **326**: 391-393 (1911).

[6] Homann F.Z., Der Einfluss Grosser Zahighkeit bei der Strmung um Den Zylinder und um Die Kugel, *Zeitschrift für Angewandte Mathematik und Mechanik,* **16**: 153-164 (1936).

[7] Howarth L., The Boundary Layer in Three Dimensional Flow. Part II. The Flow Near a Stagnation Point, *Philos. Mag.*, **42(7)**: 1433-1440 (1951).

[8] Davey A., Boundary Layer Flow at a Saddle Point of Attachment, *J. Fluid Mech.*, **10(4)**: 593-610 (1961).

[9] Wang C., Axisymmetric Stagnation Flow on a Cylinder, *Q. Appl. Math.*, **32(2)**: 207-213 (1974).

[10] Gorla R.S.R., Nonsimilar Axisymmetric Stagnation Flow on a Moving Cylinder, *Int. J. Eng. Sci.*, **16(6)**: 397-400 (1978).

[11] Gorla R.S.R., Transient Response Behaviour of an Axisymmetric Stagnation Flow on a Circular Cylinder due to Time-Dependent Free Stream Velocity, *Int. J. Eng. Sci.*, **16(7)**: 493- 502 (1978).

[12] Gorla R.S.R., Heat Transfer in Axisymmetric Stagnation Flow on a Cylinder, *Appl. Sci. Res.*, **32(5)**: 541-553 (1976).

[13] Gorla R.S.R., Unsteady Viscous Flow in the vicinity of an Axisymmetric Stagnation-Point on a Cylinder, *Int. J. Eng. Sci.*, **17(1)**: 87-93 (1979).

[14] Cunning G.M., Davis A.M.J., Weidman P.D., Radial Stagnation Flow on a Rotating Cylinder with Uniform Transpiration, *J. Eng. Math.*, **33(2)**: 113-128 (1998).

[15] Takhar H.S., Chamkha A.J., Nath G., Unsteady Axisymmetric Stagnation-Point Flow of a Viscous Fluid on a Cylinder, *Int. J. Eng. Sci.*, **37(15)**: 1943-1957 (1999).

[16] Saleh R., Rahimi A. B., Axisymmetric Stagnation-Point Flow and Heat Transfer of a Viscous Fluid on a Moving Cylinder with Time-Dependent Axial Velocity and Uniform Transpiration, *J. Fluids Eng.*, **126(6)**: 997–1005 (2004).

[17] Rahimi A. B., Saleh R., Axisymmetric Stagnation-Point Flow and Heat Transfer of a Viscous Fluid on a Rotating Cylinder with Time-Dependent Angular Velocity and Uniform Transpiration, *J. Fluids Eng.*, **129(1)**: 107–115 (2007).

[18] Rahimi A. B., Saleh R., Similarity Solution of Unaxisymmetric Heat Transfer in Stagnation-Point Flow on a Cylinder with Simultaneous Axial and Rotational Movements, *J. Heat Transfer*, **130(5)**: 054502-1–054502-5 (2008).

[19] Abbasi A. S., Rahimi A. B., Non-Axisymmetric Three-Dimensional Stagnation-Point Flow and Heat Transfer on a Flat Plate, *J. Fluids Eng.*, **131(7)**: 074501.1– 074501.5 (2009).

[20] Abbasi A. S., Rahimi A. B., Three-Dimensional Stagnation- Point Flow and Heat Transfer on a Flat Plate with Transpiration, *J. Thermophys. Heat Transfer*, **23(3)**: 513–521 (2009).

[21] Abbasi A.S., Rahimi A.B., Niazman H., Exact Solution of Three-Dimensional Unsteady Stagnation Flow on a Heated Plate, *J. Thermophys. Heat Transfer*, **25(1)**: 55–58 (2011).

[22] Abbasi A.S., Rahimi A.B., Investigation of Two-Dimensional Stagnation-Point Flow and Heat Transfer Impinging on a Flat Plate, *J. Heat Transfer*, **134(6)**: 064501-1-o64501-5 (2012).

[23] Mohammadiun H., Rahimi A.B., Stagnation-Point Flow and Heat Transfer of a Viscous, Compressible Fluid on a Cylinder, *J. Thermophys. Heat Transfer*, **26(3)**: 494-502 (2012).

[24] Mohammadiun H., Rahimi A.B., Kianifar A., Axisymmetric Stagnation-Point Flow and Heat Transfer of a Viscous Compressible Fluid on a Cylinder with Constant Heat Flux, *Sci. Iran., Trans. B*, **20(1)**: 185–194 (2013).

[25] Rahimi A.B., Mohammadiun H., Mohammadiun M., Axisymmetric Stagnation Flow and Heat Transfer of a Compressible Fluid Impinging on a Cylinder Moving Axially, *J. Heat Transfer*, **138(2)**: 022201-1-022201-9 (2016).

[26] Bejan A., Second-Law Analysis in Heat Transfer and Thermal Design, *Adv. Heat Transfer*, **15**: 1–58 (1982).

[27] Bejan A., "Entropy Generation Minimization", CRC Press, Boca Raton, Florida (1996).

[28] Bejan A., A Study of Entropy Generation in Fundamental Convective Heat Transfer, *J. Heat Transfer*, **101(4)**: 718–725 (1979).

[29] Bejan A., The Thermodynamic Design of Heat and Mass Transfer Processes and Devices, *Int. J. Heat Fluid Flow*, **8(4)**: 259-276 (1987).

[30] Mahmud S., Tasnim S. H., Mamun H. A. A., Thermodynamic Analysis of Mixed Convection in a Channel with Transverse Hydromagnetic Effect, *In. J. Therm. Sci.*, **42(8)**: 731–740 (2003).

[31] Aziz A., Entropy Generation in Pressure Gradient Assisted Couette Flow with Different Thermal Boundary Conditions, *Entropy*, **8(2)**: 50-62 (2006).

[32] Aïboud-Saouli S., Saouli S., Settou N., Meza N., Thermodynamic Analysis of Gravity-Driven Liquid Film along with an Inclined Heated Plate with Hydromagnetic and Viscous Dissipation Effects, *Entropy*, **8(4)**: 188–199 (2006).

[33] Aïboud-Saouli S., Saouli S., Settou N., Meza N., Second-Law Analysis of Laminar Fluid Flow in a Heated Channel with Hydro-Magnetic and Viscous Dissipation Effects, *Appl. Energy*, **84(3)**: 279–289 (2007).

[34] Aïboud-Saouli S., Saouli S., Entropy Analysis for Viscoelastic Magnetohydrodynamic Flow over a Stretching Surface, *International Journal of Non-Linear Mechanics*, **45(5)**: 482–489 (2010).

[35] Rezaiguia I., Mahfoud K., Kamel T., Belghar N.,. Saouli S., Numerical Simulation of the Entropy Generation in a Fluid in Forced Convection on a Plane Surface While Using the Method of Runge-Kutta, *Eur. J. Sci. Res.*, **42(4)**: 637-643 (2010).

[36] Hirschfelder J. O., Curtiss C. F., Bird, R.B, "Molecular Theory of Gases and Liquids", John Wiley & Sons, Inc., New York (1954).

[37] San J.Y., Worek W.M., Lavan Z., Entropy Generation in Combined Heat and Mass Transfer, *Int. J. Heat Mass Trans.*, **30(7)**: 1359-1369 (1987).

[38] Bianco V., Nadini S., Manca O., Enhancement of Heat Transfer and Entropy Generation Analysis of Nanofluids Turbulent Convection Flow in Square Section Tubes, *Nanoscale Res. Lett .*, **6(252)**: 1-12 (2011).

[39] Rashidi O., Mohammadi M.M., Abbasbandy F., Alhuthali, M. S., Entropy Generation Analysis for Stagnation Point Flow in a Porous Medium over a Permeable Stretching Surface, *J. Appl. Fluid Mech.*, **8(4)**: 753-765 (2015).

[40] Bejan A., Ledezma G.A., Thermodynamic Optimization of Cooling Techniques for Electronic Packages, *Int. J. Heat Mass Trans.*, **39(6)**: 1213–1221 (1996).

[41] Lin W. W., Lee D.J., Second Law Analysis of a Pin Fin Array Under Cross-Flow, *Int. J. Heat Mass Trans.*, **40(8)**: 1937–1945 (1997).

[42] Sasikumar M., Balaji C., Optimization of Convective Fin Systems: A Holistic Approach, *Heat Mass Transfer*, **39(1)**: 57–68 (2002).

[43] Rashidi M.M., Mahmud S., Freidoonimehr N., Rostami B., Analysis of Entropy Generation in an MHD Flow over a Rotating Porous Disk with Variable Physical Properties, *Int. J. Exergy*, **16(4)**: 481-503 (2015).

[44] Malvandi A., Ganji D.D., Hedayati F., Kaffash M.H., Jamshidi M., Series Solution of Entropy Generation Toward an Isothermal Flat Plate, *Thermal Science*, **16(5)**: 1289–1295 (2012).

[45] Freidoonimehr F., Rahimi A.B., Exact-Solution of Entropy Generation for MHD Nanofluid Flow Induced by a Stretching/Shrinking Sheet with Transpiration: Dual solution, *Adv. Powder Technol.*, **28(2)**: 671-685 (2017).

[46] Corcione M., Empirical correlating equations for Predicting the Effective Thermal Conductivity and Dynamic Viscosity of Nanofluids, *Ene. Convers. Manage*, **52(1)**: 789-793 (2011).

[47] Bejan M., "Entropy Generation Through Heat and Fluid Flow", John Wiley & Sons, Inc., New York, (1982).

[48] Einstein A, Eine neue Bestimmung der Molekuldimensionen , *Ann. Phys. Leipzig* **19**: 289–306 (1906).

[49] Bilal M., Sharma S., Aneja M., Cattaneo-Christov Heat Flux Model of Eyring Powell Fluid Along with Convective Boundary Conditions, *Iran. J. Chem. Chem. Eng. (IJCCE)*, **40(3)**: 971-979 (2020).

[50] Nematollahzadeh A., Jangara H., Exact Analytical and Numerical Solutions for Convective Heat Transfer in a Semi-Spherical Extended Surface with Regular Singular Points, *Iran. J. Chem. Chem. Eng. (IJCCE)*, **40(3)**: 980-989 (2020).

[51] Tiwari A. K., Pradyumna G., Jahar S., Investigation of Thermal Conductivity and Viscosity of Nanofluids, *J. Environ. Res. Develop.*, **7(2)**: 768-777 (2012).

[52] Rahimi A.B., Mohammadiun H., Mohammadiun M., Self-Similar Solution of Radial Stagnation Point Flow and Heat Transfer of a Viscous, Compressible Fluid Impinging on a Rotating Cylinder, *Iran. J. Sci. Technol. Trans. Mech. Eng.*, **43 (1)**: S141-S153 (2019).

[53] Alizadeh R., Gomari S. R., Alizadeh A., Karimi N., Li L.K.B., Combined Heat and Mass Transfer and Thermodynamic Irreversibilities in the Stagnation-Point Flow of Casson Rheological Fluid over a Cylinder with Catalytic Reactions and Inside a Porous Medium under Local Thermal Nonequilibrium, *Computers and Mathematics with Applications* (2020). [In Press].

[54] Nasir N.A. M., Ishak A., Pop I., Stagnation-Point Flow and Heat Transfer Past a Permeable Quadratically Stretching/Shrinking Sheet, *Chin. J. Phys.*, **55(5)**: 2081-2091 (2017).

[55] Thakur P., Tiwari N., Chhabra R.P., Momentum and Heat transfer from an Asymmetrically Confined Rotating Cylinder in a Power-Law Fluid, *Int. J. Therm. Sci.*, **137**: 410−430 (2019).

[56] Bayat R., Rahimi A. B., Numerical Solution of Three-Dimensional N-S Equations and Energy in the Case of Unsteady Stagnation-Point Flow on a Rotating Vertical Cylinder, *Int. J. Therm. Sci.* **118**: 386-396 (2017).

[57] Ashraf M., Ali K., Numerical Simulation of Micropolar Flow in a Channel under Osciatory Pressure Gradient**,** *Iran. J. Chem. Chem. Eng. (IJCCE)*, **39 (2)**: 261-270 (2020).

[58] Salawu S.O., Hassan A.R., Abolarinwa A., Oladejo N.K., Thermal Stability and Entropy Generation of Unsteady Reactive Hydromagnetic Powell-Eyring Fluid with Variable Electrical and Thermal Conductivities, *Alexandria Eng. J.*, **58(2)**: 519-529 (2019).

[59] Amirsom N, Uddin M. J, and Izani A, Electro Magneto Convective Stagnation Point Flow of Bionanofluid with Melting Heat Transfer and Stefan Blowing, *Thermal Science*, **22(6B)**: 2871-2881 (2018).

[60] Madelatparvar M., Hosseini Salami M., Abbasi F., Numerical Study on Parameters Affecting the Structure of Scaffolds Prepared by Freeze-Drying Method, *Iran. J. Chem. Chem. Eng. (IJCCE),* **39(2)**: 271-286 (2020).

[61] Safaei H., Sohrabi M., Falamaki C., Royaee S. J., A New Mathematical Model for the Prediction of Internal Recirculation in Impinging Streams Reactors, *Iran. J. Chem. Chem. Eng. (IJCCE),* **39(2)**: 249-259 (2020).

[62] Hussain Z., Zaman M., Nadeem M., Ullah A., CFD Modeling of the Feed Distribution System of a Gas-Solid Reactor, *Iran. J. Chem. Chem. Eng. (IJCCE),* **38(1)**: 233-242 (2019).

[63] Habibi M. R., Amini M., Arefmanesh A., Ghasemikafrudi E., Effects of Viscosity Variations on Buoyancy-Driven Flow from a Horizontal Circular Cylinder Immersed in Al_2O_3-Water Nanofluid, *Iran. J. Chem. Chem. Eng. (IJCCE),* **38(1)**: 213-232 (2019).